Supplemental Figure Legends

Figure S1. Quantitative analysis of keratocyte trajectories and simulated trajectories. *Associated with Figure 1.*
(A) Probabilities of a cell exhibiting a counter-clockwise or clockwise turning state depending on the prior turning state being counter-clockwise or clockwise as measured over 38 individual trajectories. There is no apparent memory for prior turning states in future turning states.
(B) The distribution of times between persistent turning states, measured in actual keratocyte trajectories over long observation time periods, exhibits a long-tailed distribution. Data was collected from 38 cells.
(C) Analysis of real trajectories (*top row*) and three simulated trajectories: randomly chosen angle of travel (2^{nd} *row*), randomly chosen angular speed (3^{rd} *row*), and randomly chosen change in angular speed (*bottom row*). Trajectories column shows the paths of a set of sample observed cells and one simulated trajectory from each model. Angular speed distribution column shows the count of each angular speed observed in the observed or simulated data set. Angular speed autocorrelation column shows the autocorrelation of the time series of angular speeds for a single cell's trajectory (simulated or real) plotted against the lag offset in minutes.
(D) The mean squared displacement of angular speed was calculated from the measured trajectories of cells (*left*), the simulated trajectories using randomly chosen changes in angular speed—Model C (*center*), and form the free boundary model of cell migration (*right*). Only the free boundary model was able to predict the plateau in the mean square displacement of angular speed seen in the experimental data.
(E) For 38 cells imaged over long time periods (up to 10 hours) under control conditions the average auto-correlation of angular speed at 10 minutes, $A(\omega,10min)$, the average angular speed (ω) and the average cell speed (v) were calculated for each cell. A plot of $A(\omega,10min)$ against cell speed shows that cells with more persistent turning tend to have higher cell speeds, $\rho = 0.43$, linear correlation represented by green line.
(F) Plot of $A(\omega,10min)$ against cell angular speed shows that cells with more persistent turning tend to be turning more, $\rho = 0.52$, linear correlation represented by green line.
(G) Plot of angular cell speed against cell speed shows no correlation between faster cells and cells that are turning more, $\rho = 0.11$, linear correlation represented by green line.

Figure S2. Cytoskeletal distributions in turning cells. *Associated with Figure 2*.
(A) From a collection of 707 control cells imaged twice 30 seconds apart, 195 cells imaged 8 times over 2 minutes, and 31 cells imaged every 2 seconds over 20 minutes the most significant correlations between measured parameters are presented. Green lines indicate positive correlations and red lines indicate negative correlations. Strength of correlation is represented by width of line. Spurious correlations were removed by checking for consistency with partial correlations controlling for all other variables. Shape asymmetry was not used from the 31 cells imaged over 20 minutes as left right asymmetries would average out over this length scale. Correlations were calculated from each dataset and combined linearly. Angular speed is highest amongst cells with a lower aspect ratio, these cells tend to be more disorganized at the leading edge and have slower speeds.
(B) Measurement of the distribution of actin filaments from the front/leading edge of the cell to the rear along the inner side (*green*), the center (*red*), and the outer side (*blue*) of the turning cell. Fluorescent image of F-actin distribution of a cell turning counter-clockwise, with measurement regions marked.
(C) The density of actin filaments as measured by fluorescent phalloidin stain from the front to the back of the turning cell at each of the three measurement locations as a function of the distance from the leading edge of the cell.
(D) The density of actin filaments is re-plotted as a function of time elapsed from filament formation at the leading edge [distance/speed] to give an estimate of the F-actin lifetime. Note that as a function of distance from the leading edge F-actin appears more stable on the outer wing. However, given that the there is a several-fold disparity in cell speed on the outer side versus inner side of the turning cell, the filamentous actin density on the outer wing actually drops off significantly faster as a function of time.
(E) A turning cell was permeabilized to expose the cytoskeleton, which was labeled with TMR-phalloidin and then exposed to exogenous ATP to trigger myosin contraction as described in Methods. Prior to permeabilization the cell was turning counter-clockwise (*blue path*). The first frame shows the phalloidin distribution after permeabilization and 30 seconds before addition of ATP. The second frame shows the same cell 320 seconds after exposure to ATP, with notable contraction and disassembly of the actin cytoskeleton around the cell body at the rear. The final frame shows the subtraction of these two images,

pseudo-colored to identify the regions of actin-meshwork disassembly. Disassembly was greatest on the outer side of the cell and limited at the rear of the inner side of the cell, suggesting that the asymmetry in myosin activity matches the asymmetry observed in myosin distribution. Scale bar indicates 10 microns.
(F) Outlines of the shape of a sample cell turning in the presence of 50 μM Blebbistatin. The trajectory of the cell body is marked by the dashed line in the direction of the arrowhead. With inhibition of myosin the change in orientation is directed only by polymerization at the front, which has been uncoupled from the rear. Scale bar indicates 10 microns.

Figure S3. Simulations of a turning cell with fixed shape. *Associated with Figure 4*.
(A) Schematic of the spatial distribution of adhesion strength. The two circles at the cell sides represent the regions where the adhesion strength is the highest (*red*). Adhesion strength is medium at the front (*yellow/orange*) and weakest at the rear (*blue*).
(B) Detailed simulations of cytoskeletal asymmetries in the steadily turning cell with the fixed shape. In the simulations, adhesion distribution is pre-determined and is constant in time. Myosin distribution, actin flow and traction forces are computed according to the model dynamics. Left column: adhesion (*top*) is constant. Myosin (*2nd row*) is swept by the flow to the outer side of the cell. Both actin flow (*3rd row*) and traction forces are high at the outer side of the cell. Right column: adhesion is moderate in the band along the leading edge, low at the cell rear, and high at the inner rear corner of the cell. Myosin is swept by the flow to the outer side and actin flow is high at the outer side of the cell with little change due to an asymmetric adhesion distribution. However, traction forces with an asymmetric adhesion distribution are much higher at the inner side of the turning cell, as observed in Figure 5.

Figure S4. Modeling of asymmetries in adhesion and incorporation into a comprehensive model reproducing cell turning behavior. *Associated with Figure 7*.
(A-C) For the free boundary model of cell migration the side-to-side difference in adhesion strength ($\Delta\zeta$) was fixed and in panel E the radius of curvature of the path (R), in panel F the angular velocity of the cell (ω), and in panel G the side-to-side difference in myosin concentration were calculated as the cell turned to the left. For each simulation adhesion strength at the front was either kept constant from side to side (black points), set as the left being 80% of the right (*red points*), or set as the right being 80% of the left (*blue points*). Differences of myosin concentration and adhesion strength are measured in units of average myosin concentration and adhesion strength, respectively. Note that changing adhesion strength at the leading edge made little contribution to cell turning.
(D) A plot of the assumed adhesion strength, ς, as a function of myosin concentration, M, where $\boldsymbol{\zeta = \zeta_0 \frac{M_0^2}{M_0^2+M^2}}$. Increasing myosin concentration and hence contractility is assumed to decrease the effective adhesion strength according to a non-linear stick-slip model of adhesion.
(E-H) The results of a free-boundary simulation of cell migration where cell shape and migration evolved with an initial assumption of increased adhesion strength on the left side of the cell (*pink zone*) and after 5,000 seconds with reversed adhesion asymmetry (*blue zone*). The normalized left-right asymmetry of traction forces, adhesion strength, myosin density as well as the path curvature are plotted as a time series for a single simulation in (*E*) with myosin contractility having no effect on adhesion strength, and (*F*) with increased myosin contractility negatively regulating adhesion strength. Tracks for each of these simulations are presented in (*G*) and (*H*) respectively. Each cell starts at the position marked with a red circle and migrates toward the blue arrow. Without the negative feedback of myosin contractility on adhesion strength, turning is unstable and lower in magnitude. With this negative feedback included in the simulation turning is higher in magnitude and more persistent. The normalized asymmetry is defined: $(< X_L > - < X_R >)/< X >$.
(I) Simulated trajectories of cells in an electric field under control conditions (*blue*) and with inhibition of myosin contractility (*orange)*.
(J) Summary of the models used in this manuscript.

Figure S1. Quant itative analysis of keratocyte trajectories and simulated trajectories. *Associated with Figure 1.*

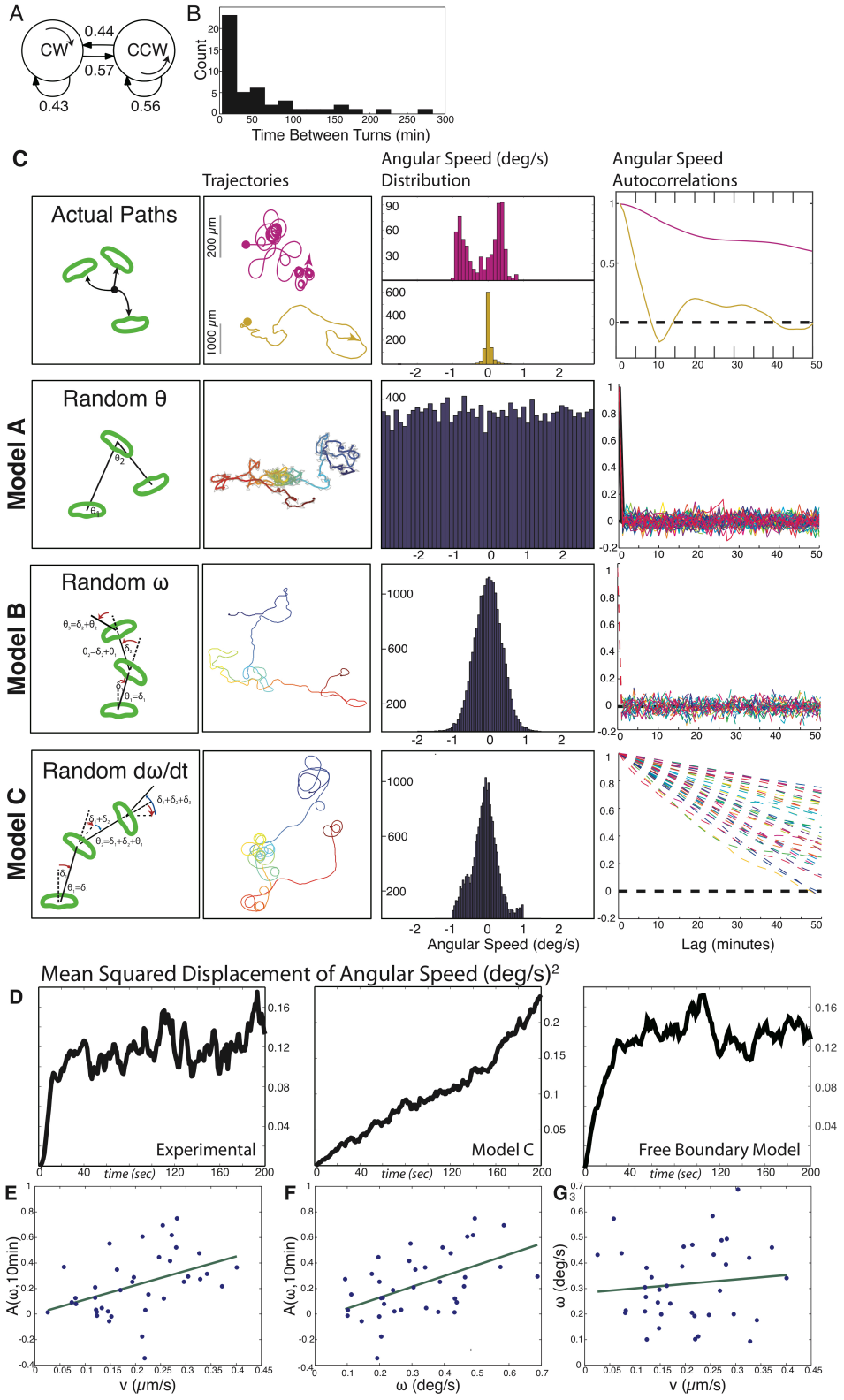

Figure S2. Cytoskeletal distributions in turning cells. *Associated with Figure 2.*

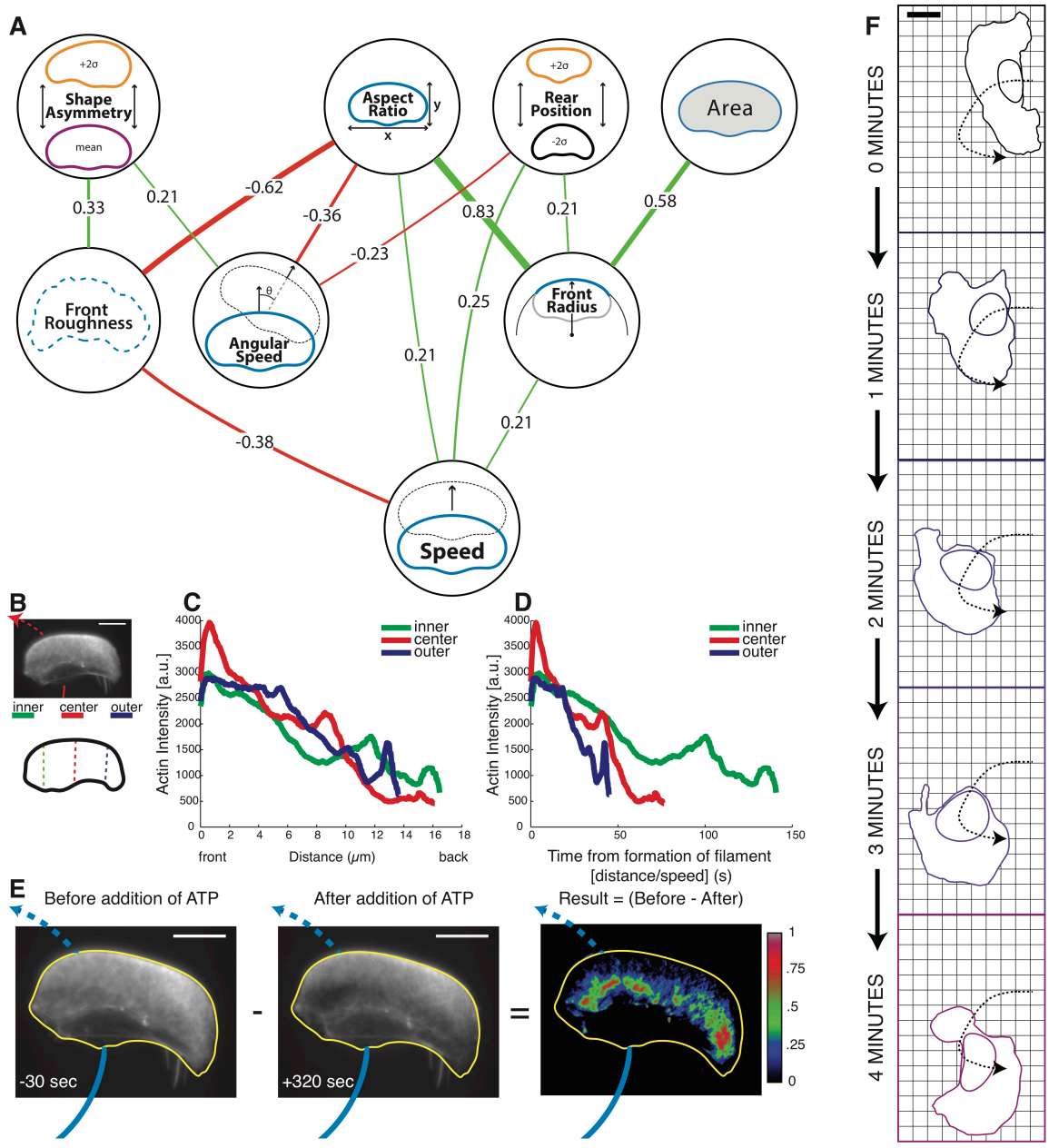

Figure S3. Simulations of a turning cell with fixed shape. *Associated with Figure 4.*

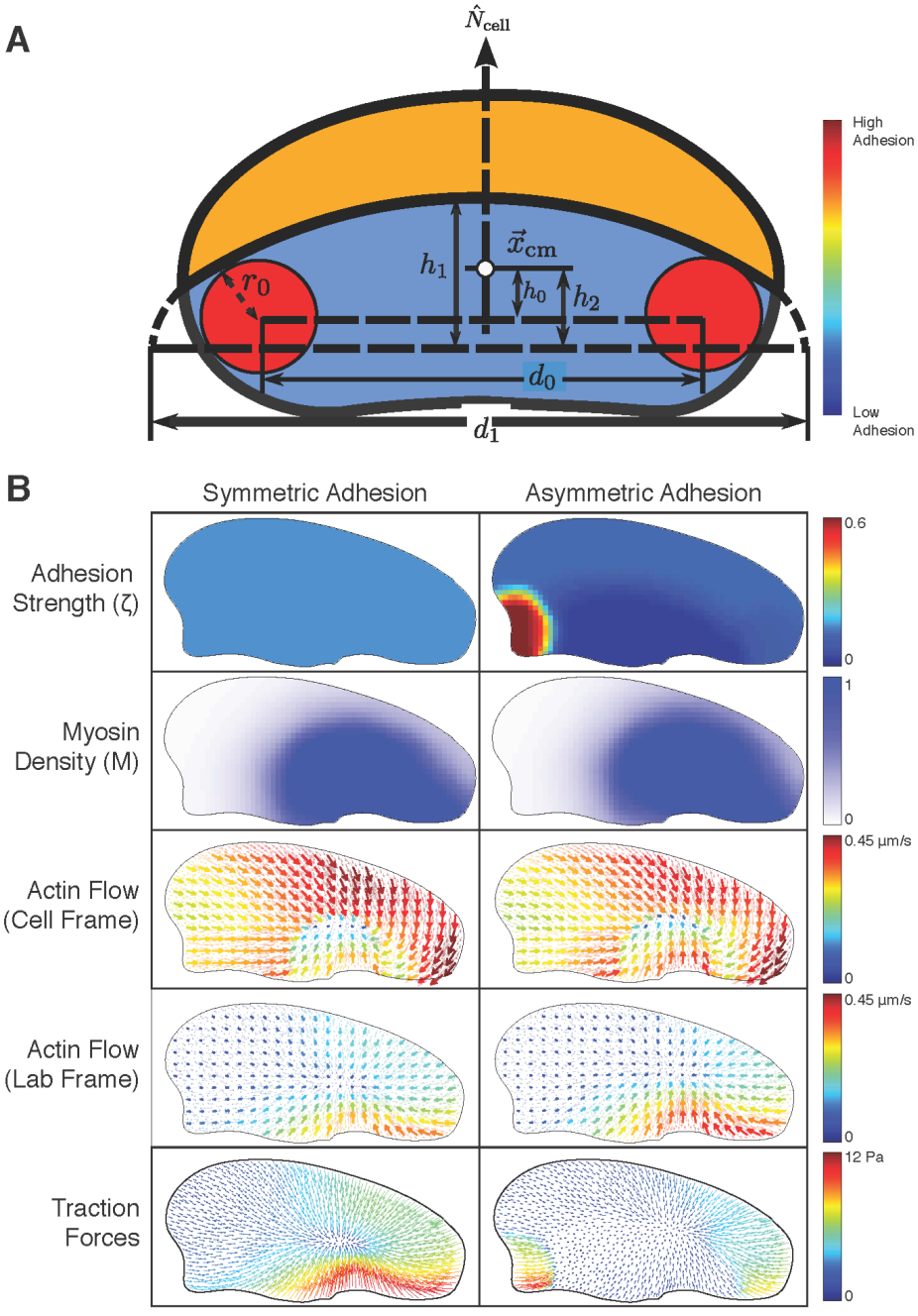

Figure S4. Modeling of asymmetries in adhesion and incorporation into a comprehensive model reproducing cell turning behavior. *Associated with Figure 7.*